Opto-Electronic Advances

Original Article

2021, Vol. 4, No. 4

DOI: 10.29026/oea.2021.210006

Diode-pumped wavelength-switchable visible Pr^{3+}:YLF laser and vortex laser around 670 nm

Xiuji Lin, Qichen Feng, Yao Zhu, Shuaihao Ji, Bo Xiao, Huiying Xu, Wensong Li* and Zhiping Cai*

Here we developed a novel wavelength-switchable visible continuous-wave (CW) Pr^{3+}:YLF laser around 670 nm. In single-wavelength laser operations, the maximum output powers of 2.60 W, 1.26 W, and 0.21 W, the maximum slope efficiencies of 34.7%, 27.3%, and 12.3% were achieved with good beam qualities (M^2 < 1.6) at 670.4 nm, 674.2 nm, and 678.9 nm, respectively. Record-high output power (2.6 W) and record-high slope efficiency (34.7%) were achieved for the Pr^{3+}:YLF laser operation at 670.4 nm. This is also the first demonstration of longer-wavelength peaks beyond 670 nm in the $^3P_1 \rightarrow {}^3F_3$ transition of Pr^{3+}:YLF. In multi-wavelength laser operations, the dual-wavelength lasings, including 670.1/674.8 nm, 670.1/679.1 nm, and 675.0/679.4 nm, were obtained by fine adjustment of one/two etalons within the cavity. Furthermore, the triple-wavelength lasings, e.g. 672.2/674.2/678.6 nm and 670.4/674.8/679.4 nm, were successfully demonstrated. Moreover, both the first-order vortex lasers (LG_0^{+1} and LG_0^{-1} modes) at 670.4 nm were obtained by off-axis pumping.

Keywords: high-power laser; visible laser; switchable laser; deep-red laser

Lin XJ, Feng QC, Zhu Y, Ji SH, Xiao B et al. Diode-pumped wavelength-switchable visible Pr^{3+}:YLF laser and vortex laser around 670 nm. *Opto-Electron Adv* **4**, 210006 (2021).

Introduction

Visible laser sources around 670 nm are in great demand in biomedical fields, such as photocoagulation[1], photothermolysis[2], hemangioma treatment[3], treatment of melasma[4], treatment of acne scars[5] and phototherapies[6–8]. Optical vortex lasers are also of great value in a wide scope of applications, especially in nanosurgery and nanomanipulation[9–11]. Benefiting from low absorption coefficients of 670 nm wavelength in some types of skin, subcutaneous, and muscle tissues[12], the 670-nm vortex laser may have the potential to manipulate particles (like erythrocytes) in these tissues.

In general, laser operations around 670 nm are generated by the conventional frequency-doubled Nd:YVO_4 lasers[13] and the AlGaInP/AlGaAs diode lasers[14]. Compared with the frequency-converted lasers, the diode-pumped solid-state lasers that can be directly generated are simple, robust, and cost-effective laser sources that can provide high laser efficiency. Owing to the inherent good beam quality, laser sources directly emitting around 670 nm also show obvious advantages over the currently available diode lasers. The Pr^{3+}:YLF crystal is a highlighted active medium for the direct generation of diode-pumped visible lasers[15–18]. This is mainly due to the fact that Pr^{3+} ions provide abundant emission lines between 500 nm and 750 nm with large peak emission cross-sections, which is typically in an order of

Department of Electronic Engineering, School of Electronic Science and Engineering (National Model Microelectronics College), Xiamen University, Xiamen 361005, China..

*Correspondence: WS Li, E-mail: wensong@xmu.edu.cn; ZP Cai, E-mail: zpcai@xmu.edu.cn

Received: 13 January 2021; Accepted: 21 March 2021; Published online: 6 April 2021

Open Access This article is licensed under a Creative Commons Attribution 4.0 International License.
To view a copy of this license, visit http://creativecommons.org/licenses/by/4.0/.

© The Author(s) 2021. Published by Institute of Optics and Electronics, Chinese Academy of Sciences.

10^{-19} cm^2 [19–20]. Nevertheless, laser operations around 670 nm based on a Pr^{3+}:YLF crystal were rarely reported[21–22], and the highest output power (0.96 W) and the highest slope efficiency (12.7%) achieved so far were relatively low. Therefore, we proposed a novel wavelength-switchable continuous-wave (CW) visible Pr^{3+}:YLF lasers around 670 nm. Record-high output power (2.6 W) and record-high slope efficiency (34.7%) were achieved for the π-polarized laser operation at 670.4 nm, which were more than two times higher than the values reported before. With two etalons inserted into the cavity, the single-wavelength σ-polarized lasings at 674.2 nm and 678.9 nm were realized for the first time, and high output powers of 1.26 W and 0.21 W were achieved with high slope efficiencies of 27.3% and 12.3%, respectively. At all three wavelengths, the beam qualities of the proposed lasers were competitive with all the M^2 factors in the horizontal (x) and the vertical (y) directions below 1.6. Multi-wavelength laser operations around 670 nm were also obtained by both etalons combinations. Furthermore, visible first-order vortex lasers (both LG_0^{+1} and LG_0^{-1} modes) at 670.4 nm were firstly obtained by off-axis pumping. We believe such a novel visible laser around 670 nm could provide cost-effective techniques for emerging biomedical applications.

Experimental setup

As shown in Fig. 1, a commercial InGaN laser diode (LD) array emitting at ~444 nm with the maximum output power of 24 W was applied as the pump source. To reduce the spherical aberration and make the focusing spot of the pump beam smaller, an aspherical plane-convex lens with a focal length of 75 mm was used to focus the pump light. A simple end-pumped plane-concave laser cavity with the insertion of one/two etalons (i.e., Etalon-1 and/or Etalon-2) was constructed to obtain the wavelength-switchable laser operation. The input coupler (IM) was based on a coated plane mirror, which has a high reflectivity (>99.9%) at 665–700 nm and high transmissions at 600–639 nm. A piece of 100 mm radius-of-curvature plane-concave mirror with transmissivities of 0.3% at 670 nm, 0.5% at 675 nm, and 0.9% at 679 nm was applied as the output coupler (OC). It is worth pointing out that the transmission of the OC at 698 nm is over 60%, and can effectively prevent the available optical gain from lasing. The etalons are made of optical glass BK7. The thickness of Etalon-1 is 100 μm, and it was inserted at the Brewster angle to suppress the π-polarized emissions. Another three pieces of Etalon-2 with different thicknesses of 100 μm, 150 μm, and 200 μm were vertically inserted into the cavity and tilted to achieve wavelength-switchable laser oscillations.

A commercial fabricated a-cut Pr^{3+}:YLF crystal employed for the following experiments has a low Pr^{3+} doping ratio of 0.12 at. %, the length of 15 mm, and 3 mm × 3 mm polished facets without anti-reflection coating. To protect the crystal from thermally induced fragmentation, we wrapped the crystal with indium foil and placed it in a water-cooled copper crystal holder. The temperature of the cooling water was set to 13 °C. A wide ~2.2 nm of full width at half maximum (FWHM) of the pump laser spectrum leads to a relatively low absorption efficiency ~51% of the Pr^{3+}:YLF crystal. Here ~10% loss of pump laser power was introduced by the plane-convex lens and the plane mirror (i.e., IM). The physical cavity length was optimized to be 53 mm. It should be noted that the performance of the single-wavelength 670.4 nm laser was optimized with a concave-plane cavity (to reduce thermal effects) with the same cavity parameters, rather than the above-described plane-concave cavity.

Results and discussion

Visible single-wavelength laser operation

Figure 2 presented the experimental results of the single-wavelength laser operation around 670 nm. The maximum output powers of 2.60 W, 1.26 W, and 0.21 W with the maximum slope efficiencies of 34.7%, 27.3%, and 12.3% were achieved at 670.4 nm, 674.2 nm, and 678.9 nm, respectively. Firstly, laser oscillation at π-polarized 670.4 nm was obtained by the concave-plane cavity

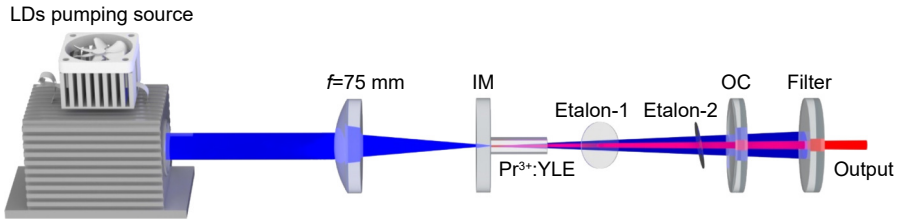

Fig. 1 | Schematic of the diode-pumped wavelength-switchable CW visible Pr^{3+}: YLF laser around 670 nm

above-mentioned without etalons. To obtain single-wavelength operations at two σ-polarized wavelengths, Etalon-1 was inserted into the cavity at the Brewster angle to suppress emission at π-polarized 670.4 nm. Meanwhile, two pieces of Etalon-2 with thicknesses of 100 μm and 150 μm were vertically inserted into the cavity to obtain lasing at 674.2 and 678.9 nm, respectively. The laser spectra were measured by a spectrometer (Ocean Optics, HR4000+). Due to the relatively low resolution (0.3 nm), the linewidths appeared to be a bit large. Since the YLF crystal generally exhibits negative thermal lensing effects[23], the mode volume of the laser in the gain medium will be enlarged in a plane-concave or a concave-plane cavity as the thermal lensing effects become strong. Thus, the laser slope efficiency can increase under high-power pumping due to the increment of overlap efficiency, as detailedly shown in Fig. 2(a). Three single-wavelength lasing spectra were given in Fig. 2(b). Correspondingly, the beam qualities of the single-wavelength lasers were also characterized in Fig. 2(c), including 670.4 nm laser with 1.2 and 1.4 in the x and y directions, respectively; 674.2-nm laser with 1.5 and 1.4 in the x and y directions, respectively; 678.9-nm laser with 1.4 and 1.4 in the x and y directions, respectively. The M^2 factor was calculated through $M^2 = \theta\pi w_0/\lambda$ (ISO 11146), where θ is the divergence half-angle, w_0 is the beam waist radius, and λ is the laser wavelength. Power stabilities of these single-wavelength lasers are presented in Fig. 2(d). Due to the relatively low absolute output power as well as the noises from the environment and the thermal power meter (Thorlabs S425C-L, detection sensitivity > 2 mW), the power stability of the 678.9-nm laser appeared to be little higher. Wavelength drift was not observed during the power stability measuring. Here the polarization directions of these single-wavelength lasers, i.e., 670.4 nm in π-polarization,

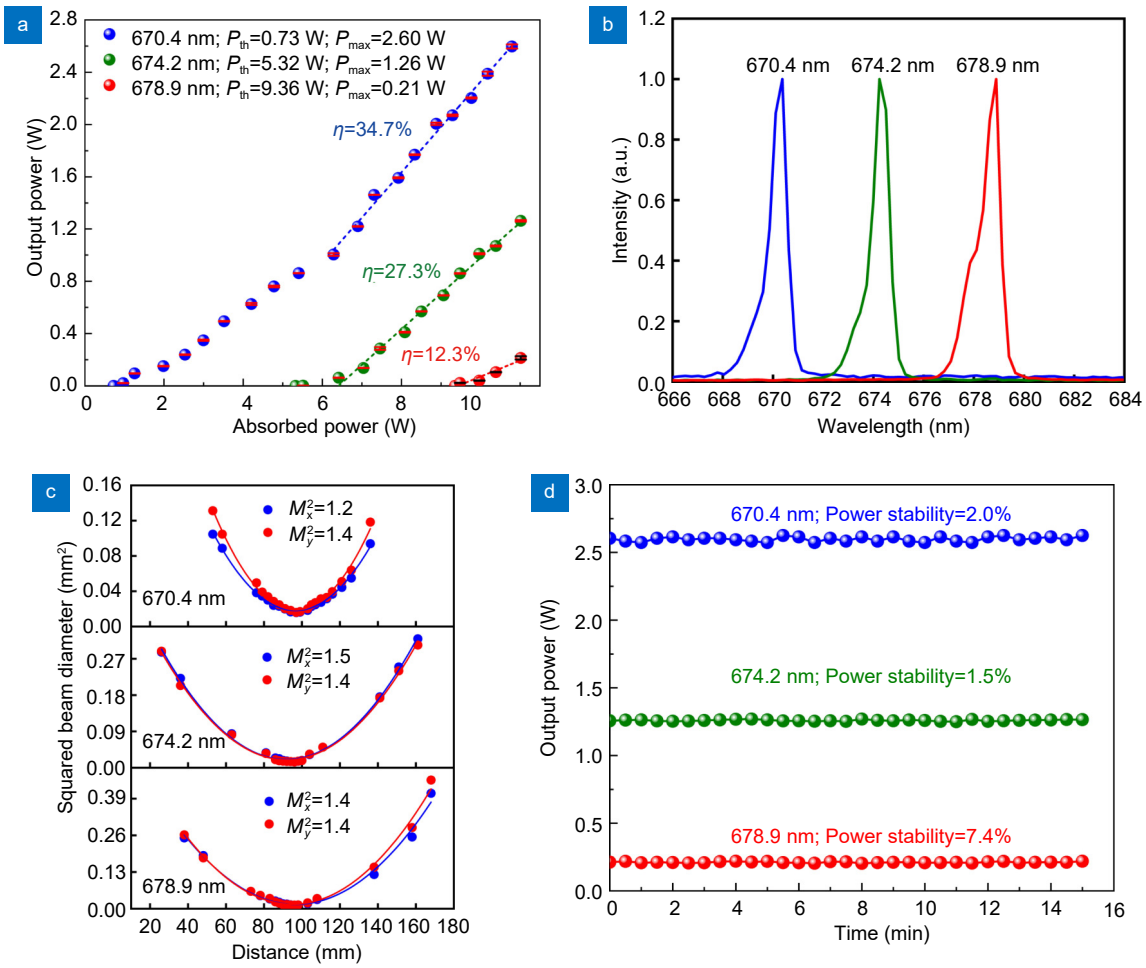

Fig. 2 | Experimental results of single-wavelength lasers around 670 nm. (**a**) Output powers and slope efficiencies with respect to absorbed pump powers. (**b**) Laser output spectra at 670.4 nm, 674.2 nm, and 678.9 nm, respectively. (**c**) Measured corresponding M^2 factors of 670.4 nm, 674.2 nm, and 678.9 nm, respectively. (**d**) Power stabilities of lasers at 670.4 nm, 674.2 nm, and 678.9 nm

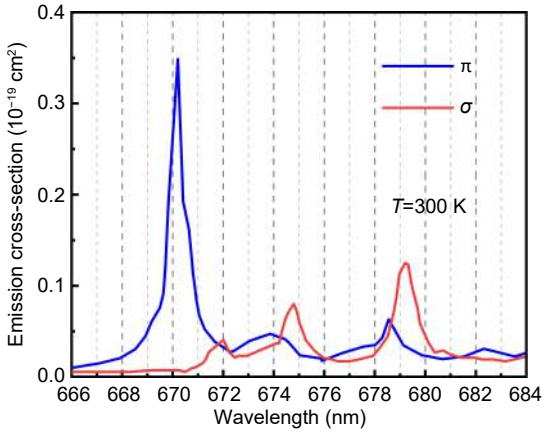

Fig. 3 | Emission cross sections of Pr^{3+}:YLF crystal around 670 nm under room temperature.

and both 674.2 nm and 678.9 nm in σ-polarization, were confirmed by a Glan–Taylor prism. The polarization results we obtained were coincident with the spectroscopy characteristics around 670 nm (see Fig. 3).

To further understand the high-power and high-efficiency performance under high-power pumping conditions, simulations of the 670-nm laser with different beam radius (affected by the thermal lensing effects) were carried out. The input-output power characteristics can be expressed by[24] (the spatial distribution is expressed under a normal cartesian coordinate system; z is the direction perpendicular to the facets of the crystal)

$$P_{\rm in}=\frac{A_{\rm e}\gamma I_{\rm sat}}{\eta_{\rm p}}\left[\int_a\frac{\varepsilon\left(x,y,z\right)g\left(x,y,z\right)}{\left(2P_{\rm out}/TA_{\rm e}I_{\rm sat}\right)\varepsilon\left(x,y,z\right)+1}{\rm d}V\right]^{-1}, \tag{1}$$

where $P_{\rm out}$ is the output power; $P_{\rm in}$ is the input power; $A_{\rm e}$ is the effective mode area; γ is the total logarithmic single-pass loss; $I_{\rm sat}$ is the saturation intensity; η_p can be treated as the Stokes efficiency (because we used the absorbed power in the simulation and we assumed that the optical transfer efficiency is one); $g(x,y,z)$ is the normalized pump distribution inside the crystal; $\varepsilon(x,y,z)$ is the dimensional mode distribution factor of the laser (the specific definition of the $g(x,y,z)$ and the $\varepsilon(x,y,z)$ can be found in ref.[24]); T is the power transmissivity at the wavelength of the laser; the integral symbol and the dV means the integration of the whole space. For a circular Gaussian beam, the $\varepsilon(x,y,z)$ can be written as

$${\rm e}^{\frac{-2(x^2+y^2)}{w_{\rm l}^2}}, \tag{2}$$

where $w_{\rm l}$ is the radius of the laser beam. Since the Rayleigh distance is much longer than the length of the crystal in this cavity scheme, the variation of the beam radius along the z direction can be reasonably neglected. Due to the different pump beam sizes and M^2 factors in the x and y directions, the pump beam can be approximately described as an elliptical Gaussian beam. Thus, the $g(x,y,z)$ can be written as

$$\frac{2\alpha\beta_{\rm pe}}{\pi\bar{w}_{\rm pe}^2\left(1-{\rm e}^{-\alpha l}\right)}{\rm e}^{-2\left(\frac{\beta_{\rm pe}^2x^2+y^2}{\bar{w}_{\rm pe}^2}\right)-\alpha z}, \tag{3}$$

where α is the absorption efficiency; $\beta_{\rm pe}$ is the ratio of minor to major beam size; $\bar{w}_{\rm pe}$ is the average beam radius in the minor direction; l is the length of the active medium. Then the input-output power characteristics with different laser beam sizes can be calculated. The results were presented in Fig. 4 and the parameters for the simulation were listed in Table 1. As can be seen from Fig. 4, the slope efficiency became higher while the laser beam size became larger. The simulation results obtained can clearly explain the rising trend of the slope efficiency of the experimental results. Compared with that of the previous works on 670-nm lasers[21–22], the high-power and high-efficiency results were achieved because, except for the advantages brought by the thermal lensing effects mentioned above, we did not use the etalon to obtain the lasers at 670 nm. Since the power transmissivity of the OC at 670 nm is quite low, the total single-pass loss (γ) is very sensitive to the intracavity losses. As can be seen from Eq. (1), the $P_{\rm in}$ is very sensitive to the γ when the other parameters remain unchanged. Thus, the elimination of the intracavity losses introduced by the etalon is also very critical to achieve high output power and high slope efficiency (at 670 nm).

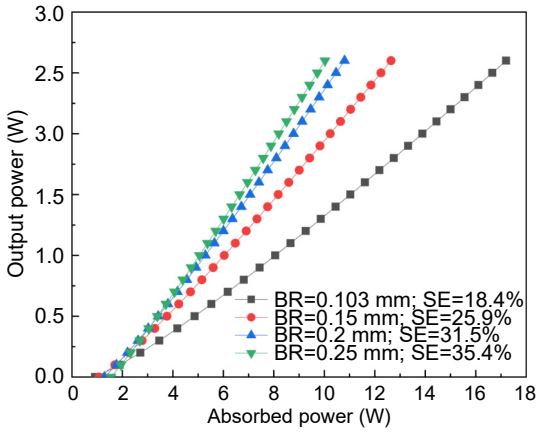

Fig. 4 | Simulation results of the input-output power characteristics at 670 nm. BR is the waist beam radius of the laser; SE is the slope efficiency. 0.103 mm is the smallest beam radius which can be obtained by the cavity parameters.

Table 1 | Parameters used in the simulation. $2\gamma_{in}$ is the total intracavity logarithmic round-pass loss.

α (mm^{-1})	$\bar{w}_{pe}$(mm)	T(%)	$2\gamma_{in}$	I_{sat}(W/mm^2)	λ (mm)	β_{pe}	l(mm)
0.0476	0.173	0.3	0.002	1694.2	6.7×10^{-4}	0.391	15

Visible multi-wavelength laser operation

Multi-wavelength laser oscillations around 670 nm were achieved by tilting the crystal and inserting the etalons with different thicknesses. As shown in Fig. 5, laser performances of the multi-wavelength operation were characterized. By slightly tilting the YLF crystal to adjust the intracavity losses, the maximum output power of 2.52 W was achieved at dual-wavelength 670.1/674.8 nm (see Fig. 5(a)). But notably, such a dual-wavelength operation only appeared under high-power pumping (i.e., over 10 W of absorbed pump power). The dual-wavelength laser at 675.0/679.4 with the maximum output power of 1.80 W and the maximum slope efficiency of 34.1% was achieved by inserting the etalon-1 with 100 μm thickness at the Brewster angle. And the dual-wavelength laser at 670.1/679.1 nm with the maximum output power of 0.36 W was achieved by vertically inserting the Etalon-2 with 200-μm thickness and then tilting it finely.

Figure 5(b) shows the dual-wavelength laser spectra at 670.1/674.8, 670.1/679.1, and 675.0/679.4, respectively. The intensities of these pairwise lasers in the dual-wavelength operations were comparable, which implied the potential of obtaining a higher power laser at ~679 nm with suitable etalons to match the emission peak. Then, as seen in Fig. 5(c), two types of triple-wavelength laser operations were also achieved. The triple-wavelength laser at 670.4/674.8/679.4 nm with output power of 1.78 W was obtained by tilting the crystal, and it only appeared at the available highest pumping. The triple-wavelength laser at 672.2/674.2/678.6 nm with the maximum output power of 0.84 W also only appeared under the available highest pumping, but it was achieved by inserting both Etalon-1 with 100-μm thickness and Etalon-2 with 150-μm thickness. Power stabilities of these multi-wavelength lasers are presented in Figs. 5(d) and 5(e). Due to the mode competition, the stabilities of the multi-wavelength lasers are generally worse than the single-wavelength lasers. Wavelength drift was not observed during the output power stability measuring.

The power transmission of the etalon can be expressed by[25]

$$T = \frac{1}{1 + \frac{4R}{(1-R)^2}\sin^2\left(\frac{2\pi}{\lambda} nd\cos\theta\right)}, \tag{4}$$

where T is the power transmissivities; R is the reflectivity of the surface (~0.04 in our schemes); n is the refractive index of the glass (~1.51 at 675 nm); d is the thickness of the etalon; θ is the angle between the rays and the normal to the reflective faces. According to Eq. (4), the tilting angle of the etalons can be estimated (the main deviation was introduced by the resolution of the spectrometer we used). For example, for the dual-wavelength laser at 670.1/679.1 nm, when the angle of the etalon with a 200-μm thickness was tilted to 1.68°, the power transmissivities were over 99.8% at 670.1 and 679.1 nm as well as only 85.2% at 674.2 nm. Similar analyses can also be applied to other tuning results, including the single-wavelength results in the above section.

Visible vortex laser operation

A visible vortex laser at 670.4 nm was obtained by using an off-axis pumping technique. The laser cavity was designed as the concave-plane one above-mentioned. By carefully rotating the plane mirror in x and y directions, two diagonal Hermite-Gaussian (HG) 01 modes could be obtained because the threshold of the fundamental mode could exceed the HG_{01} mode under off-axis conditions. Then, two diagonal HG_{01} modes at 3π/4 and π/4 angles (relative to the horizontal direction) could form the Laguerre-Gaussian (LG) mode with an introduced Gouy phase of π/2[26]. As known, such a hollow beam could be coherently or incoherently superposed by two diagonal beams[27]. Thus, it's necessary to verify the phase of the wavefront (helical or not) and rotate the plane mirror repeatedly. This step is the main challenge to obtain vortex laser. As seen in Fig. 6(a), the maximum output power of 0.23 W with a slope efficiency of 10.8% was obtained. By slightly moving the crystal perpendicularly to the propagation direction of the laser, both the first-order vortex lasers (LG_0^{+1} and LG_0^{-1} modes) were realized. The output power characteristics of both modes are almost the same. The beam patterns of the vortex lasers were measured by a charge-coupled device (CCD) placed after the OC (the distance between the OC and the CCD is ~30 mm). When the absorbed pump power was over

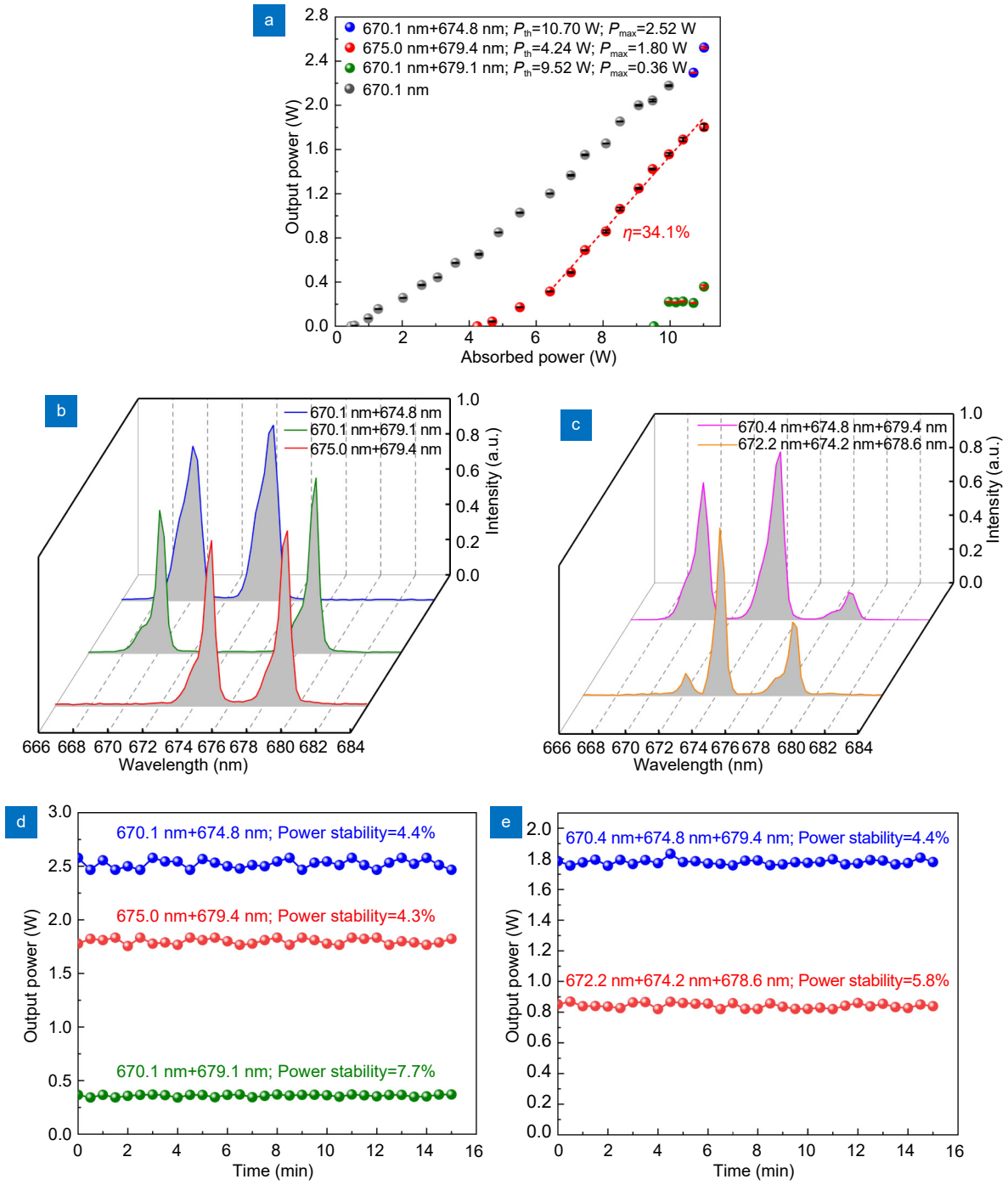

Fig. 5 | (**a**) Output characteristics of dual-wavelength lasers around 670 nm, i.e., 670.1/674.8, 670.1/679.1, 675.0/679.4 nm, respectively. (**b**) Laser output spectra of dual-wavelength lasers measured at the maximum output powers of 2.52, 1.80, and 0.36 W, respectively. (**c**) Laser output spectra of triple-wavelength lasers measured at the output powers of 1.78 and 0.84 W, respectively. (**d**) Power stabilities of the dual-wavelength lasers. (**e**) Power stabilities of the triple-wavelength lasers.

2.9 W, the lasers did not sustain vortical forms because the increased thermal lensing effects might break the mode-matching conditions of the first order LG modes. Under high-power pumping, it is challenging to meet the mode-matching conditions of the vortex laser in the π direction due to the larger thermo-optic coefficient (compared with the σ direction) and the complex spatial distribution of the pump beam. To verify the vortex operations, a plane-concave mirror with a high reflective dielectric coating at ~670 nm on the concave surface was applied as an improved Fizeau interferometer[28] to get the interference patterns. Figure 6(b) presents the vortex

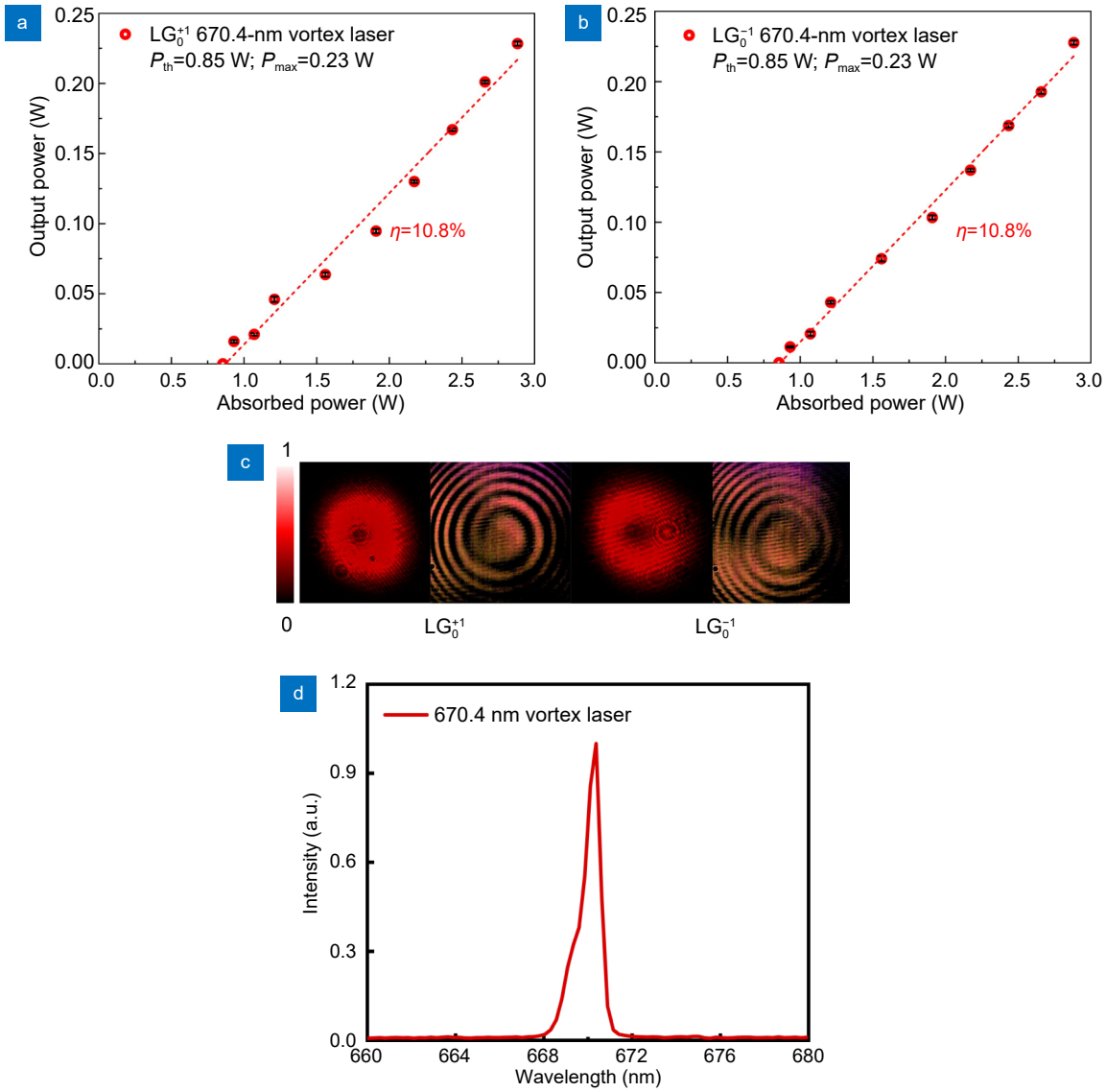

Fig. 6 | (**a**) Output performance of the visible vortex laser at 670.4 nm (LG_0^{+1} and LG_0^{-1} modes). (**b**) Measured laser beam spots and the corresponding spiral interference patterns. (**c**) Laser spectrum of the vortex lasers (the spectra of the different LG modes were the same).

laser beam spots and the corresponding spiral interference patterns. The specific scheme of verification can be found in our previous work on vortex laser[29].

Conclusions

A novel wavelength switching of CW visible Pr^{3+}:YLF laser was demonstrated around 670 nm. The maximum output power of 2.60 W and the maximum slope efficiency of 34.7% obtained for a single-wavelength laser at 670.4 nm are the highest values so far. Single-wavelength laser operations at 674.2 nm and 678.9 nm were demonstrated for the first time. Investigated good beam qualities with M^2 below 1.6 contribute to the practical applications. Multi-wavelength laser operations are characterized by the dual-wavelength lasings (i.e., 670.1/674.8 nm, 670.1/679.1 nm, and 675.0/679.4 nm, respectively) and the triple-wavelength lasings (i.e., 672.2/674.2/678.6 nm and 670.4/674.8/679.4 nm, respectively). Moreover, the visible vortex laser at 670.4 nm was also realized for the first time. Such a novel wavelength-switchable visible laser and vortex laser around 670 nm could open up new horizons for the practical applications in biophotonics fields. Though the high-power lasers around 670 nm were obtained, OCs with different transmissions at this wavelength region were not yet explored since there are no available mirrors in our lab. Other tuning methods are worth trying to obtain broader and continuous tuning since the free spectrum range of the etalon is quite narrow. Besides, the reason for the unsustainable vortex laser under high-power pumping should be studied in

details in the future to propose more rational schemes to obtain higher output power.

References

1. Immonen I, Viherkoski E, Peyman GA. Experimental retinal and ciliary body photocoagulation using a new 670-nm diode laser. *Am J Ophthalmol* **122**, 870–874 (1996).
2. Müller A, Marschall S, Jensen OB, Fricke J, Wenzel H et al. Diode laser based light sources for biomedical applications. *Laser Photon Rev* **7**, 605–627 (2013).
3. Genovese WJ, dos Santos MTBR, Faloppa F, de Souza Merli LA. The use of surgical diode laser in oral hemangioma: a case report. *Photomed Laser Surg* **28**, 147–151 (2010).
4. Nisticò SP, Tolone M, Zingoni T, Tamburi F, Scali E et al. A new 675 nm laser device in the treatment of melasma: results of a prospective observational study. *Photobiomodul Photomed Laser Surg* **38**, 560–564 (2020).
5. Cannarozzo G, Silvestri M, Tamburi F, Sicilia C, Del Duca E et al. A new 675-nm laser device in the treatment of acne scars: an observational study. *Lasers Med Sci* **36**, 227–231 (2021).
6. Yeager RL, Franzosa JA, Millsap DS, Angell-Yeager JL, Heise SS et al. Effects of 670-nm phototherapy on development. *Photomed Laser Surg* **23**, 268–272 (2005).
7. Sommer AP, Bieschke J, Friedrich RP, Zhu D, Wanker EE et al. 670 nm laser light and EGCG complementarily reduce amyloid-β aggregates in human neuroblastoma cells: basis for treatment of Alzheimer's disease? *Photomed Laser Surg* **30**, 54–60 (2012).
8. Noudeh YJ, Shabani M, Vatankhah N, Hashemian SJ, Akbari K. A combination of 670 nm and 810 nm diode lasers for wound healing acceleration in diabetic rats. *Photomed Laser Surg* **28**, 621–627 (2010).
9. Jeffries GDM, Edgar JS, Zhao YQ, Shelby JP, Fong C et al. Using polarization-shaped optical vortex traps for single-cell nanosurgery. *Nano Lett* **7**, 415–420 (2007).
10. Ashkin A, Dziedzic JM. Optical trapping and manipulation of viruses and bacteria. *Science* **235**, 1517–1520 (1987).
11. Maruyama H, Kotani K, Masuda T, Honda A, Takahata T et al. Nanomanipulation of single influenza virus using dielectrophoretic concentration and optical tweezers for single virus infection to a specific cell on a microfluidic chip. *Microfluid Nanofluid* **10**, 1109–1117 (2011).
12. Bashkatov AN, Genina EA, Tuchin VV. Optical properties of skin, subcutaneous, and muscle tissues: a review. *J Innov Opt Health Sci* **4**, 9–38 (2011).
13. Yao AY, Hou W, Bi Y, Geng AC, Lin XC et al. High-power cw 671 nm output by intracavity frequency doubling of a double-end-pumped Nd:YVO4 laser. *Appl Opt* **44**, 7156–7160 (2005).
14. Schneider RP, Choquette KD, Lott JA, Lear KL, Figiel JJ et al. Efficient room-temperature continuous-wave AlGaInP/AlGaAs visible (670 nm) vertical-cavity surface-emitting laser diodes. *IEEE Photonics Technol Lett* **6**, 313–316 (1994).
15. Metz PW, Reichert F, Moglia F, Müller S, Marzahl DT et al. High-power red, orange, and green Pr^{3+}:$LiYF_4$ lasers. *Opt Lett* **39**, 3193–3196 (2014).
16. Luo SY, Yan XG, Cui Q, Xu B, Xu HY et al. Power scaling of blue-diode-pumped Pr:YLF lasers at 523.0, 604.1, 606.9, 639.4, 697.8 and 720.9 nm. *Opt Commun* **380**, 357–360 (2016).
17. Tanaka H, Fujita S, Kannari F. High-power visibly emitting Pr^{3+}:YLF laser end pumped by single-emitter or fiber-coupled GaN blue laser diodes. *Appl Opt* **57**, 5923–5928 (2018).
18. Lin XJ, Zhu Y, Ji SH, Li WS, Xu HY et al. Highly efficient LD-pumped 607 nm high-power CW Pr^{3+}:YLF lasers. *Opt Laser Technol* **129**, 106281 (2020).
19. Kränkel C, Marzahl DT, Moglia F, Huber G, Metz PW. Out of the blue: semiconductor laser pumped visible rare-earth doped lasers. *Laser Photonics Rev* **10**, 548–568 (2016).
20. Chen HJ, Uehara H, Kawase H, Yasuhara R. Efficient Pr:YAlO3 lasers at 622 nm, 662 nm, and 747 nm pumped by semiconductor laser at 488 nm. *Opt Express* **28**, 3017–3024 (2020).
21. Qu B, Xu B, Luo SY, Cheng YJ, Xu HY et al. InGaN-LD-Pumped continuous-wave deep red laser at 670 nm in Pr^{3+}:$LiYF_4$ crystal. *IEEE Photonics Technol Lett* **27**, 333–335 (2015).
22. Qu B, Huang Q. Watt-level diode-pumped continuous-wave Pr:$LiYF_4$ laser at 670 nm and simultaneous dual-wavelength operation at 639 and 670 nm. *Appl Opt* **59**, 3033–3037 (2020).
23. Hardman PJ, Clarkson WA, Friel GJ, Pollnau M, Hanna DC. Energy-transfer upconversion and thermal lensing in high-power end-pumped Nd:YLF laser crystals. *IEEE J Quantum Electron* **35**, 647–655 (1999).
24. Laporta P, Brussard M. Design criteria for mode size optimization in diode-pumped solid-state lasers. *IEEE J Quantum Electron* **27**, 2319–2326 (1991).
25. Rust DM. Étalon filters. *Opt Eng* **33**, 3342–3348 (1994).
26. Beijersbergen MW, Allen L, van der Veen HELO, Woerdman JP. Astigmatic laser mode converters and transfer of orbital angular momentum. *Opt Commun* **96**, 123–132 (1993).
27. Kim DJ, Kim JW. Direct generation of an optical vortex beam in a single-frequency Nd:YVO4 laser. *Opt Lett* **40**, 399–402 (2015).
28. Cui SW, Xu B, Luo SY, Xu HY, Cai ZP et al. Determining topological charge based on an improved Fizeau interferometer. *Opt Express* **27**, 12774–12779 (2019).
29. Lin XJ, Cui SW, Ji SH, Tian QY, Zhu Y et al. LD-pumped high-power high-efficiency orange vortex Pr^{3+}:YLF lasers. *Opt Laser Technol* **133**, 106571 (2021).

Acknowledgements

This work was supported by the National Natural Science Foundation of China (Nos. 11674269, 61975168).

Competing interests

The authors declare no competing financial interests.